ACS OMEGA

Open Access

http://pubs.acs.org/journal/acsodf

Article

Significantly Tunable Foaming Behavior of Blowing Agent for the Polyethylene Foam Resin with a Unique Designed Blowing Agent System

Xuelian Chen* and Qigu Huang*

Cite This: *ACS Omega* 2024, 9, 5798−5808

Read Online

ACCESS | Metrics & More | Article Recommendations | Supporting Information

ABSTRACT: The chemical blowing agent plays a crucial role in enhancing the performance of the polyethylene (PE) foaming resin during the rotational foaming process. Previously, the conventional blowing agent of the PE resin commonly used pure azodicarbonamide (AZ). It had the unavoidable drawbacks of releasing NH_3 and exhibiting strong reactions during the rotational foaming process. Meantime, pure AZ had a relatively high decomposition temperature, resulting in a sharp foaming process. To address the above issues, this work developed a uniquely designed blowing agent system. In this study, a novel blowing agent for the PE resin was successfully synthesized by a one-pot method. This blowing agent consisted of an activator and AZ, which exhibited a lower decomposition temperature and a milder decomposition rate than AZ. The activator was constituted of small-sized ammonium dihydrogen phosphate on the AZ surface, which could be decomposed properly and deliver phosphoric acid and H_2O during the foaming process. Then, AZ reacted with H_2O under phosphoric acid catalysis. Also, this reaction generated CO_2 emission while reducing the emission of NH_3 through recombination with phosphoric acid. Moreover, phosphoric acid catalysis caused a decrease in the AZ decomposition temperature. Meantime, the thermal coupling appeared during the foaming process, which could further reduce the decomposition rate. Consequently, the small activator played a key role in regulating cell formation and diffusion. Compared to AZ, the novel blowing agent system significantly reduced the cell diameter of the PE foam resin and enhanced its flexural modulus by 50%. Furthermore, the novel blowing agent facilitated better demolding performance and improved the surface morphology of the PE foam product. This research provides significant foaming behavior regulation for the PE resin during industrial applications.

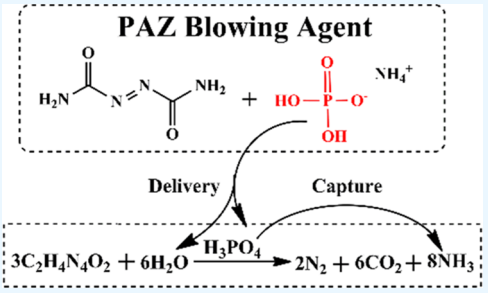

1. INTRODUCTION

Polyethylene (PE) is a commonly used plastic material with a wide range of applications.[1−9] The research studies of PE have also received extensive attention for its synthesis,[10] modification,[11−13] application,[14−16] degradation,[17,18] etc. Foaming technology has been widely applied in PE products, such as injection foaming and rotational foaming.[19−21] The foaming behavior directly affects the performance of the PE foaming products. Therefore, the regulation of foaming behavior is a highly important and valuable research work.

For rotational molding, it is currently a terrific technique used to create large hollow plastic products in the plastic industry. This method is favored for its ability to minimize residual stress, cost-effective molds, and the opportunity for intricate structural designs.[22] With the continuous growth of the economy, applications of rotational molding have expanded significantly. It is now utilized in various industries such as the military, chemistry for containers, recreation facilities, marine facilities, sports products, and medical devices.[23,24] Building upon the principles of rotational molding, the rotational foaming technology was developed, which shares the benefits of rotational molding and introduces additional features like sandwich-structure products with multiple layers.[25−29] Notably, polyethylene (PE) and polyurethane (PU) are the primary products for rotational foaming. In general, PU foam in rotational foaming products is limited to being used as a filler. This is because it is challenging to fill larger and more complex products, leading to delamination with the outer layer. On the other hand, the PE foam for sandwich-structure products provides better adhesion between the core and skin layers. The foaming process of PE foam products involves the introduction or generation of gases within the polymer matrix. These gases can be produced using either a physical or chemical blowing agent.[30,31] For blowing agent comparison, only chemical blowing agents can be used in rotational foaming due to atmospheric operation. Physical blowing agents would increase mold pressure, resulting in higher equipment costs.[32] Therefore,

Received: November 3, 2023
Revised: January 13, 2024
Accepted: January 16, 2024
Published: January 29, 2024

compared with physical blowing agents, chemical blowing agents offer more convenience in the rotational foaming process.

Increased attention has been given by researchers to studying the mechanisms of the rotational foaming process.[33−41] The foaming process consists of four distinct stages: primary nucleation, secondary nucleation, bubble growth, and bubble shrinkage. Notably, it was discovered that primary nucleation occurred in interstitial regions, which has a significant role in determining the final cellular structure. Additionally, secondary nucleation takes place within the polymer melt.[33] The influence of polymeric viscosity on the nucleation rate was also investigated by using modified nucleation theory. Also, the experimental data served as a verification for this theory.[34−36] For various PE foam products, such as linear low-density polyethylene (LLDPE), high-density polyethylene (HDPE), and their blends, a comprehensive analysis of cellular structures utilized noninvasive X-ray microcomputed tomography. The results demonstrated that microcells usually have a tendency to grow and elongate in the thickness direction.[37] The duration of the bubble lifespan is greatly influenced by the processing temperature, diffusivity, and gas bulk concentration. To account for these effects, a mathematical model was employed, considering factors such as diffusion, surface tension, viscosity, and elasticity. Additionally, it was observed that an increase in the chemical blowing agent content led to a higher number of cells being nucleated. Also, the particle size of the chemical blowing agent impacted the bubble's lifespan.[38,39] Utilizing an optical microscope, the decomposition behavior of the chemical blowing agent and the zero-shear viscosity of LLDPEs during foaming were examined. It was determined that the content of the chemical blowing agent, processing temperature, and heating time played vital roles in the cell morphology. Further, the performance of the chemical blowing agent strongly influenced the foaming properties. The foaming behavior of the chemical blowing agent was the key for PE foam products, such as decomposition temperature, decomposition rate, and the generated gas.[40,41] There is a lack of specific chemical blowing agents designed for the rotational foaming process of the PE resin. Moreover, the conventional blowing agent azodicarbonamide (AZ) possesses a higher decomposition temperature and faster decomposition rate for the PE resin.[32] Consequently, several challenges arise in PE rotational foaming with an AZ blowing agent. First, the melting point temperature of PE resin is relatively low. Also, pure AZ requires a high decomposition and foaming temperature. This incongruity makes it unsuitable for the slow heating process of the inner surface during rotational molding. Furthermore, the heating process for rotational foaming requires significantly more time compared with injection molding or blow molding. The prolonged rotational molding cycle is caused by the temperature difference between the inner and outer surfaces of the products. The exothermic reaction leads to an increasingly faster decomposition rate of the AZ thermal decomposition. As a result, there is a defect of large-sized cells on the outer surface of the PE foam product, potentially leading to combustion. Additionally, an incomplete foaming process appears on the inner surface of the PE resin, which can adversely affect the PE foam product performance. Moreover, the exothermic reaction of AZ decomposition gives rise to some secondary reactions and generates low-molecular-weight compounds such as biurea, urazol, and cyanic acid. Cyanic acid further exacerbates the issue.[42,43] These reactions often lead to the PE foam product sticking to the mold, compromising the product quality. In summary, a specialized blowing agent for PE resin is an urgent requirement in rotational foaming. It is significant that AZ as a blowing agent is replaced by the novel blowing agent to ensure optimal performance and quality of the PE foam product.

In this work, a novel blowing agent was synthesized by a one-pot method. This blowing agent consisted of an activator and AZ, which exhibited a lower decomposition temperature and a milder decomposition rate than AZ. The activator was constituted of small-sized ammonium dihydrogen phosphate on the AZ surface, which could be decomposed properly and deliver phosphoric acid and H_2O during the foaming process. Then, AZ reacted with H_2O under phosphoric acid catalysis. Also, this reaction generated CO_2 while reducing the emission of NH_3 through recombination with phosphoric acid. Moreover, phosphoric acid catalysis caused a decrease in the AZ decomposition temperature. Meantime, the thermal coupling appeared during the foaming process, which could further reduce the decomposition rate. Also, it demonstrated notable enhancement in the flexural modulus of PE foam products by utilizing the novel blowing agent instead of AZ.

2. EXPERIMENTAL SECTION

2.1. Materials. The supplied PE resin material had a melt index of 8.0 g/10 min as per ASTM D1238, using a 2.16 kg load under a temperature of 190 °C. This material was provided by Shenhua (Beijing) New Materials Company. The chemical blowing agent AZ refers to a commercially available azodicarbonamide obtained from Adamas Reagent Co., Ltd. The particle size range of the industrial AZ grade varied from 12 to 18 μm, with an average particle size of approximately 13 μm. Another chemical blowing agent, known as OBSH, was also purchased from Adamas Reagent Co., Ltd. For the experiment, a phosphoric acid reagent with a purity level exceeding 98% was obtained from J&K Scientific Company. ZnO was acquired from Sinopharm Group Reagent Co., Ltd. $NH_3{\cdot}H_2O$, which is a 25 wt % ammonia solution in H_2O, was procured from Aladdin as an analytical purity product.

2.2. Equipment and Characterization. The rotational molding machine used in this study was a shuttle machine labeled F01−1000, provided by Yantai Fangda Corporation in China. The inner diameter of the machine's oven was 1.0 m. The twin-screw extruder utilized had a diameter of 26 mm and an L/R ratio of 40. X-ray diffraction (XRD) analysis was performed at room temperature by using a Bruker D8 ADVANE instrument. The XRD measurements employed 0.154 nm Cu target rays, scanning within the range 10−80° at 2θ with a voltage of 40 kV and a current of 40 mA. The scanning step size was 0.02°, while the residence time was 0.2 s per step. The ATR-FTIR spectra were acquired on a Shimadzu Prestige-21 IR Prestige-21 spectrophotometer. Additionally, a thermogravimetric analysis machine-coded TGA 1550, obtained from Thermo Fisher, was used. The thermoanalytical experiment involved increasing the sample temperature at a heating rate of 10 °C/min under a nitrogen atmosphere. Cellular morphology observation of PE foam product was carried out employing a computer imaging stereoscopic microscope XTL-24BC, purchased from Shanghai Pudan Optical Instruments Co., Ltd. Microstructural analysis was conducted by using Nova Nano SEM 450, manufactured by the FEI company. Finally, the flexural modulus was determined through testing conducted with an Instron 5965 apparatus.

2.3. Preparation of the Novel Blowing Agent of PAZ. To synthesize the novel blowing agent, 1.16 g of AZ foaming agent was dissolved in 20 mL of deionized (DI) water. The

https://doi.org/10.1021/acsomega.3c08734
ACS Omega 2024, 9, 5798−5808

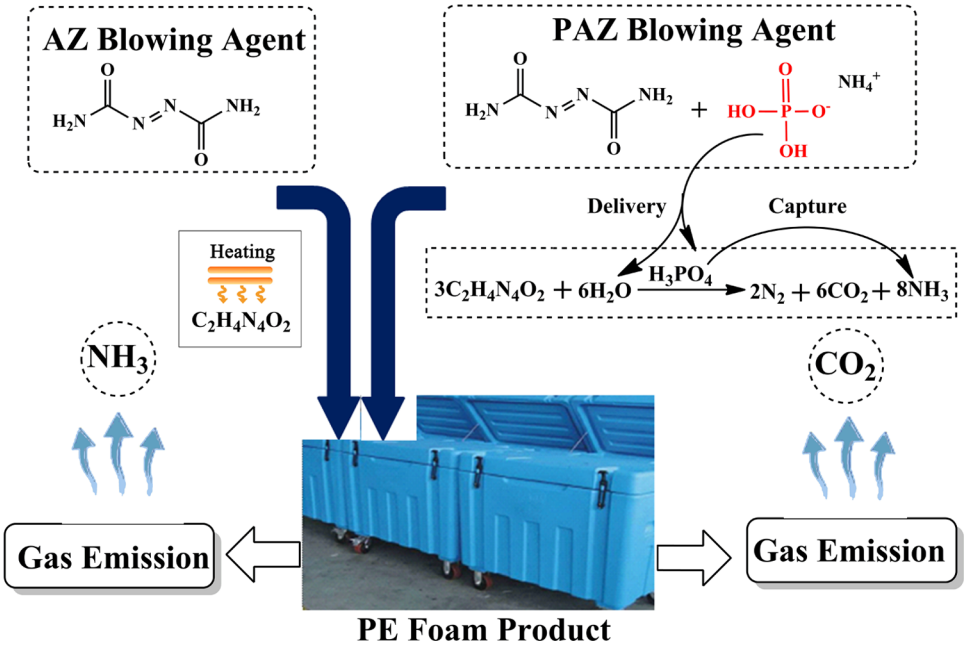

Figure 1. Schematic illustration of the individual foaming mechanisms for AZ and PAZ during the PE foaming process.

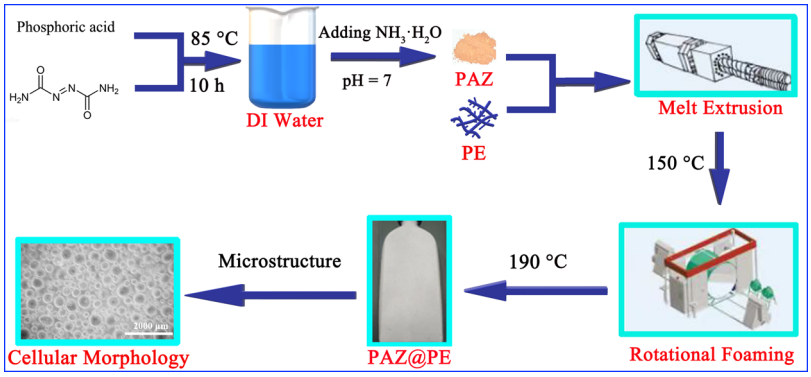

Figure 2. Preparation process of the PE foam product by rotational foaming with PAZ.

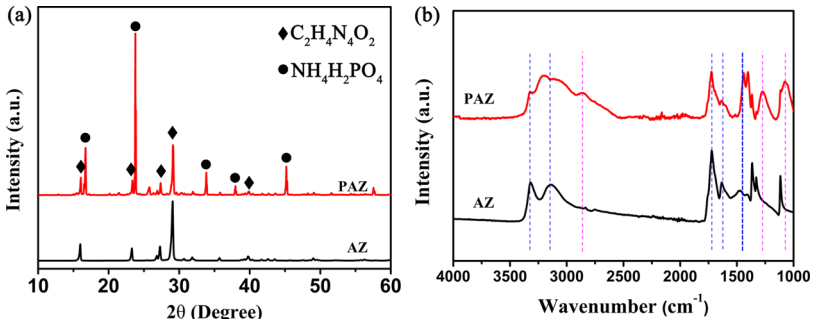

Figure 3. (a) XRD patterns and (b) FTIR spectra of the pure AZ and PAZ samples.

solution was then heated to 85 °C and stirred for 8 h. Subsequently, 7.84 g of phosphoric acid was introduced, and the resulting mixture was stirred for approximately 10 h. Next, $NH_3 \cdot H_2O$ was employed to adjust the pH to 7. The solution was subsequently subjected to vacuum drying at 50 °C for 12 h. The resulting product was identified as the novel blowing agent, designated as PAZ. The foaming mechanisms for AZ and PAZ are illustrated in Figure 1. During the process of PE foaming, the main released gas was NH_3 by thermal decomposition of the AZ blowing agent. On the other hand, the PAZ blowing agent was composed of AZ and an activator. The activator consisted of small-sized ammonium dihydrogen phosphate on the surface of AZ, delivering phosphoric acid and H_2O during the PE foaming process. Under the catalysis of phosphoric acid, AZ reacted with H_2O. This reaction mainly resulted in the emission of plenty of CO_2 and small amounts of N_2. Also, it simultaneously reduced the emission of NH_3 by phosphoric acid absorption.

https://doi.org/10.1021/acsomega.3c08734
ACS Omega 2024, 9, 5798−5808

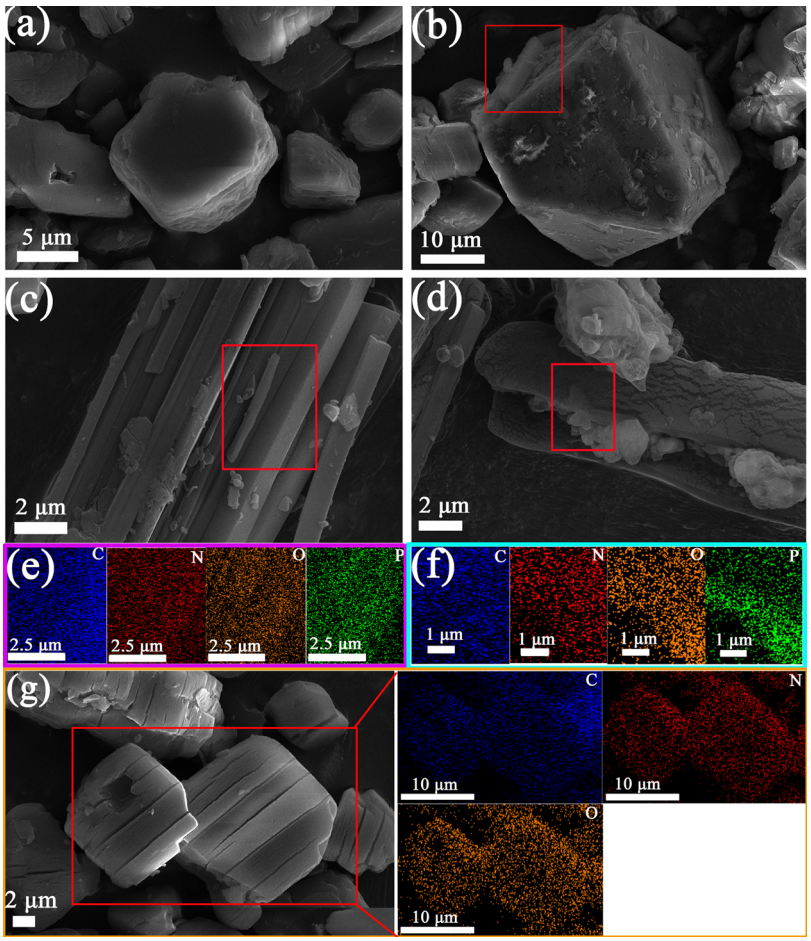

Figure 4. SEM images of (a) AZ and (b–d) PAZ. EDS elemental mapping of (e, f) PAZ. (g) SEM image and EDS elemental mapping of PAZ washed by DI water.

2.4. Preparation of the PE Foam Product by Rotational Molding. The melt mixtures of PE and a chemical blowing agent were prepared by using a twin-screw extruder at a temperature of 150 °C. It is important to note that the processing temperature should be maintained above the melt temperature of the PE resin and below the decomposition temperature of the chemical blowing agent. Subsequently, the mixtures of PE resin and the chemical blowing agent were ground into a powder, which was then utilized in the subsequent rotational foaming process. The experimental mold size for this study was 450 mm × 370 mm × 200 mm. The temperature for the rotational foaming process was determined based on the characteristics of the mixtures. The oven temperature could be adjusted according to the demand. The heating time for both blends was set at 24 min, with the spindle and secondary shaft speeds set to 5 and 8 rpm, respectively. The resulting PE foam products with AZ and PAZ were denoted as AZ@PE and PAZ@PE, respectively. Figure 2 depicts the process of the PE foam product obtained through rotational foaming using PAZ as the blowing agent.

3. RESULTS AND DISCUSSION

3.1. Characterization of PAZ. The XRD analysis in Figure 3a revealed the crystal structures of pure AZ and PAZ. The XRD pattern of the pure AZ sample matched the structure of azodicarbonamide ($C_2H_4N_4O_2$) (PDF No. 28−1535) with characteristic peaks at 16.0, 23.3, 27.4, 29.0, and 41.7°. Importantly, the XRD pattern of PAZ closely resembled that of AZ, confirming the presence of azodicarbonamide as one of the main crystalline materials. Additionally, the XRD peaks of PAZ at 16.7, 23.9, 33.9, 37.9, and 45.1° corresponded to the structure of ammonium dihydrogen phosphate ($NH_4H_2PO_4$) (PDF No. 85−0815). Both AZ and ammonium dihydrogen phosphate diffraction peaks were observed in the PAZ sample, indicating the presence of numerous ammonium dihydrogen phosphate particles. Moreover, the characteristic peaks of ammonium dihydrogen phosphate in the PAZ sample were stronger than those of AZ, which implied the presence of plenty of small-sized ammonium dihydrogen phosphate particles on the surface deposition of large-sized AZ particles.

As demonstrated in Figure 3b, the characteristic absorption peak of PAZ at 1475 cm^{-1} noticeably declined. This decline might be attributed to the abundant formation and dispersion of ammonium dihydrogen phosphate on the surface of the AZ particles. Additionally, the distinctive bimodal structure of pure AZ sample at 3000−3300 cm^{-1} was replaced by a wide absorption peak ranging from 2500 to 3300 cm^{-1}. It also provided the corresponding evidence. Furthermore, the presence of the −P−O-H, −P═O, and −P−O functional groups displayed the novel absorption peaks observed at 2856, 1250, and 1060 cm^{-1}, respectively. Therefore, the characteristic absorption peaks of PAZ confirmed the formation of ammonium dihydrogen phosphate. These findings are consistent with the XRD results.

https://doi.org/10.1021/acsomega.3c08734
ACS Omega 2024, 9, 5798−5808

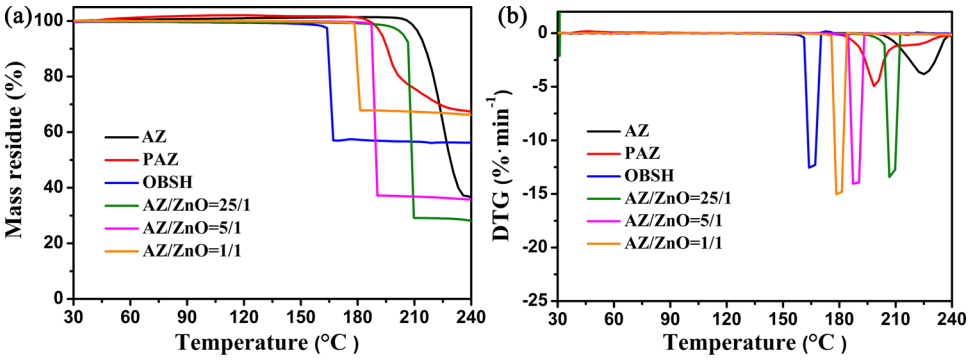

Figure 5. (a) TG and (b) DTG curves of different samples for comparison.

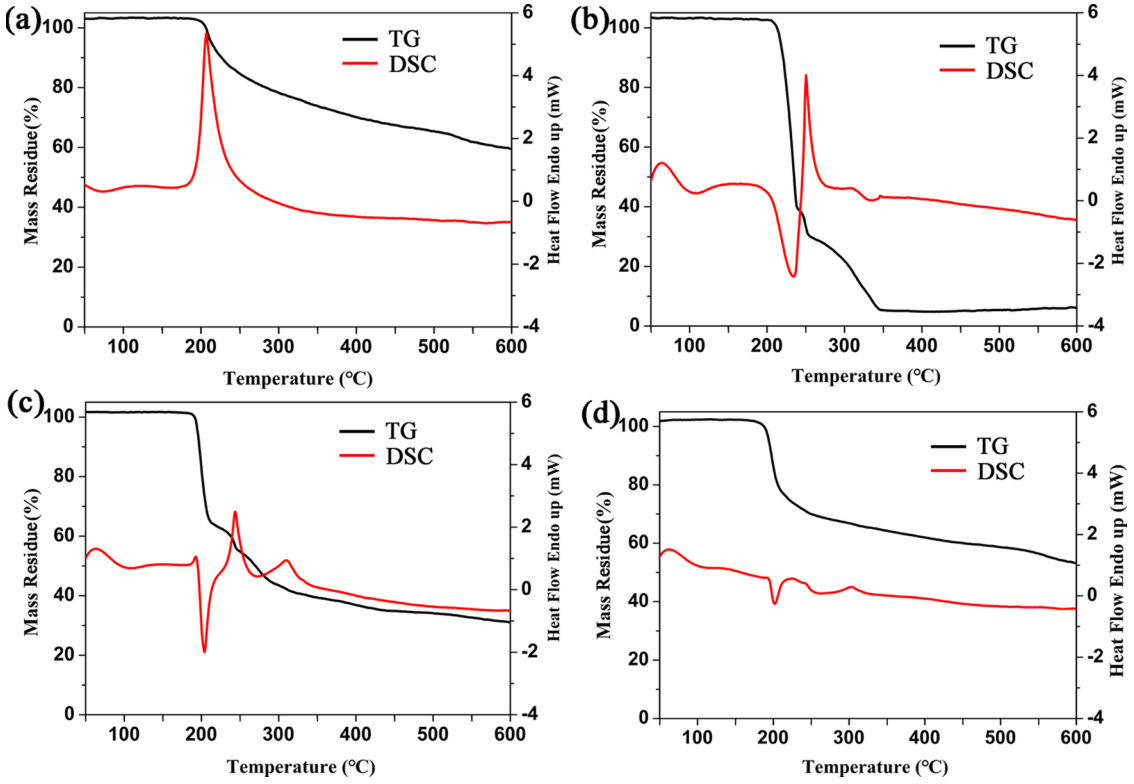

Figure 6. TG and DSC curves of (a) $NH_4H_2PO_4$, (b) AZ, (c) PAZ-1 ($NH_4H_2PO_4$:AZ = 1:1), and (d) PAZ-2 ($NH_4H_2PO_4$:AZ = 2:1).

The scanning electron microscopy (SEM) technique was used to further analyze the detailed morphologies of AZ and PAZ. SEM images of AZ are shown in Figure 4a, revealing that the majority of AZ particles had an irregular shape with a rough and cracked surface. The size of the particles was relatively uniform, with a diameter below 40 μm. In contrast, the morphology of PAZ differed from that of AZ. Figure 4b exhibits a distinctive prismatic structure on the surface of AZ particles, indicated by the red square. Additionally, numerous small particles were observed on the particle surface, forming intimate interfaces. Figure 4c displays a large number of prismatic crystals. Also, Figure 4d reveals a significant aggregation of small-sized particles. Figure 4e shows the corresponding elemental mapping in the red square of Figure 4c, highlighting the presence of C, N, O, and P elements. Similarly, Figure 4f provides the elemental mapping in the red square of Figure 4d, confirming the presence of C, N, O, and P elements. These observations suggested that the PAZ sample contained two types of morphologies dispersed on the surface of AZ particles. In comparison, Figure 4g demonstrates the SEM image of PAZ after being washed with DI water, indicating the absence of small particles and prismatic crystals on the particle surface of the AZ particles. The corresponding elemental mapping of the red square in Figure 4g comprises only C, N, and O elements. Also, the P element was not observed, consistent with FTIR spectral results (Figure S1). It indicated that ammonium dihydrogen phosphate could be easily washed away from PAZ by DI water.

3.2. Thermal Decomposition Performance of PAZ. For the blowing agent of the PE foam product, the optimal temperature range for the initial decomposition in the rotational foaming process is crucial. A lower initial decomposition temperature may result in the blowing agent decomposing before the PE resin is fully melted. It results in the decomposition gas of the blowing agent being released prematurely and wasted rapidly. Conversely, when the blowing agent had a higher initial decomposition temperature, an excessive decomposition rate can cause uneven cell distribution in the inner and outer layers of PE foam products during the

https://doi.org/10.1021/acsomega.3c08734
ACS Omega 2024, 9, 5798−5808

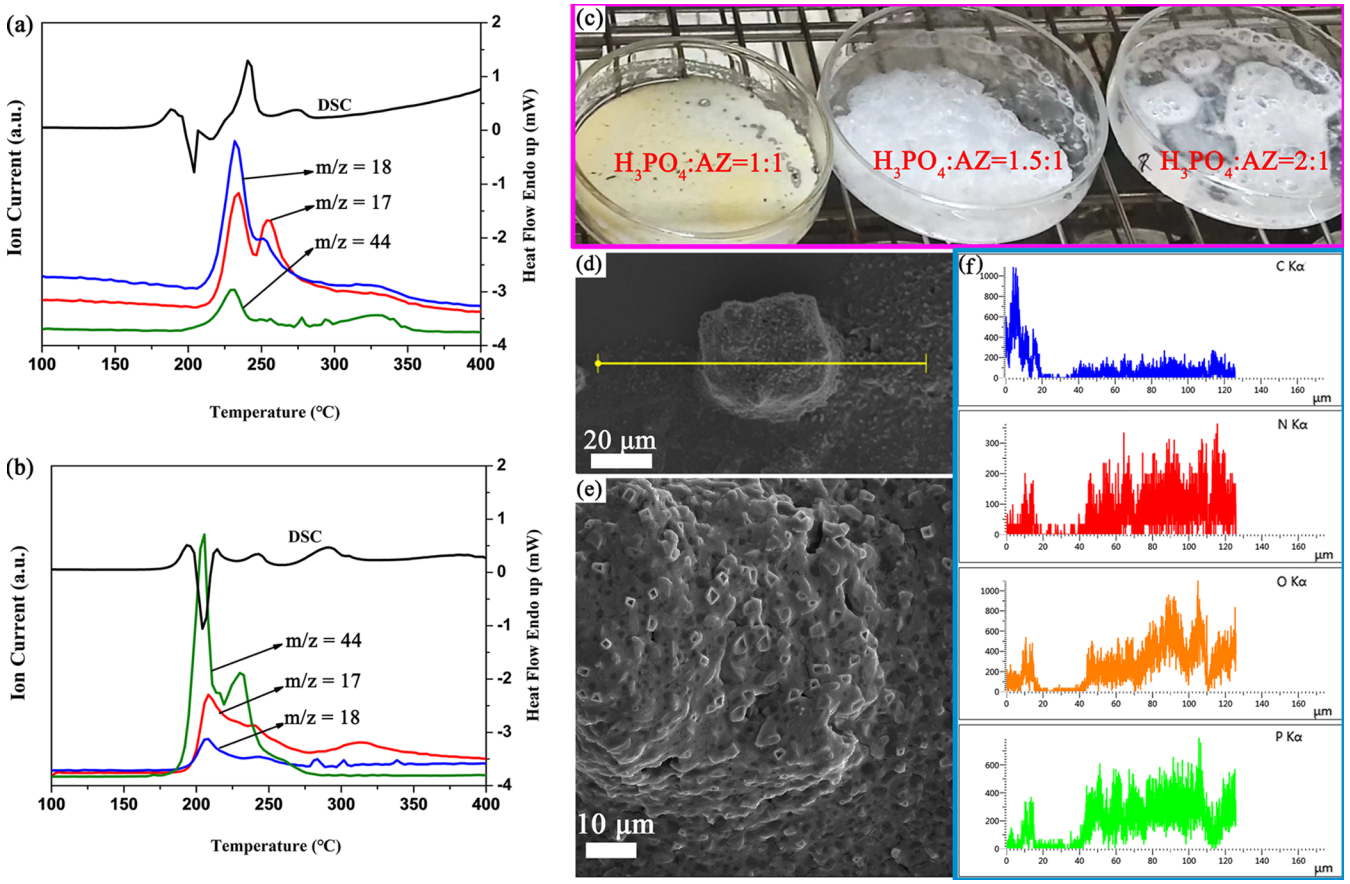

Figure 7. DSC and mass spectrometric intensity curves during the thermal decomposition of (a) AZ and (b) PAZ. (c) Photographs of AZ with H_2O decomposition reaction during the heating process at 120 °C by adding H_3PO_4. (d,e) SEM images of the sample with the mole ratio of H_3PO_4:AZ = 1:1 after the decomposition reaction. (f) EDS spectra of the sample with the mole ratio of H_3PO_4:AZ = 1:1 after the decomposition reaction.

rotational foaming process. Therefore, the thermal decomposition characteristics of PAZ played a crucial role, including its thermal decomposition temperature and rate.

TG analysis was utilized to measure the thermal decomposition characteristics of the samples. As illustrated in Figure 5a, PAZ exhibited a lower initial decomposition temperature, nearly being at 180 °C compared with AZ, nearly being at 210 °C. Additionally, the PAZ blowing agent system exhibited a higher residual mass after thermal decomposition. It is advantageous that the PAZ system has a high ash content because bubble nucleation preferentially occurs on the small-sized solid particles. Additionally, the initial decomposition temperature of pure OBSH is as low as 165 °C, which has an improper low initial decomposition temperature for PE resin. Especially, for the AZ/ZnO blowing agent system, the initial decomposition temperature decreases significantly with the increase of the ZnO loading dose. The initial thermal decomposition temperature of the AZ/ZnO blowing agent system decreased significantly compared with that of pure AZ. For the thermal decomposition temperature rate, the PAZ blowing agent system exhibited a more favorable rate compared with the AZ/ZnO and OBSH blowing agent systems (Figure 5b). The moderate decomposition rate of PAZ also facilitated the nucleation growth of primary bubbles and resulted in a smaller average cell size during the rotational foaming process. Unlike the existing blowing agent systems involving AZ with heavy metal salts, metal oxides, and other activators, the PAZ blowing agent system is a uniquely designed system that operates on a novel foaming mechanism.[44,45]

For the thermal effect aspect, the thermal decomposition reaction of pure ammonium dihydrogen phosphate was unmistakably endothermic, as depicted in Figure 6a. It exhibited an initial decomposition temperature of 180 °C and reached its peak temperature at 204 °C. As displayed in Figure 6b, the thermal decomposition of pure AZ showed an exothermic peak at 236 °C, followed by an endothermic peak at 251 °C. For the PAZ blowing agent system, PAZ-1 demonstrated an intriguing offsetting phenomenon between exothermic and endothermic reactions. This phenomenon suggested that the presence of ammonium dihydrogen phosphate as an activator influenced the thermal decomposition behavior of AZ (Figure 6c). More importantly, Figure 6d illustrates that PAZ-2 exhibits a regulated exothermic reaction through the thermal coupling effect. This effect proved advantageous for PE foam products in achieving a reduced average cell diameter during the rotational foaming process.

For the gaseous products of thermal decomposition, the gases released from AZ and PAZ were carefully recorded, respectively. The results of this analysis can be observed in Figure 7a,b, respectively. As depicted in Figure 7a, the mass spectrometric intensity curves displayed distinct ion fragments with m/z values of 17, 18, and 44, corresponding to NH_3 and CO_2. It was evident that the primary released gas during the thermal decomposition of AZ was NH_3 above 210 °C, aligning with the main reaction stage observed in the DSC spectrum. In contrast, Figure 7b

https://doi.org/10.1021/acsomega.3c08734
ACS Omega 2024, 9, 5798−5808

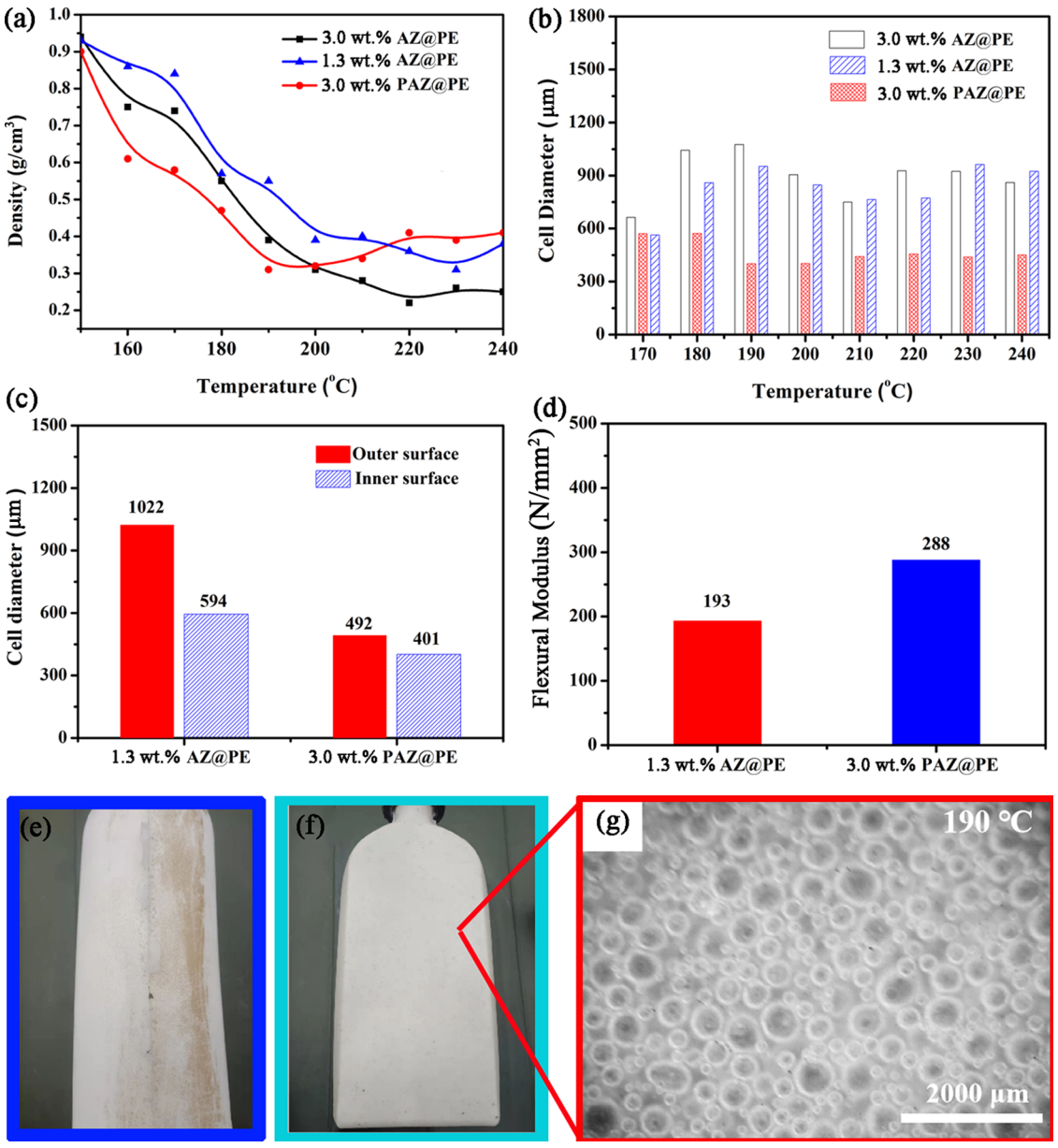

Figure 8. (a) Density curves. (b) Histograms of cell diameter. (c) Cell diameters of the inner and outer surfaces. (d) Flexural modulus of the samples. PE foam product images of (e) 1.3 wt % AZ@PE and (f) 3.0 wt % PAZ@PE. (g) Cell morphology image of 3.0 wt % PAZ@PE at 190 °C.

illustrates that the primary released gas during the thermal decomposition of PAZ was CO_2 above 180 °C, differing significantly from the decomposition process of AZ. The decomposition behavior of PAZ can be described as follows: (i) An initial decomposition temperature of 180 °C indicated the initial pyrolysis of ammonium dihydrogen phosphate, resulting in the generation of diammonium dihydrogen diphosphate ($(NH_4)_2H_2P_2O_7$), H_2O, NH_3, and phosphoric acid (H_3PO_4) (reactions 1 and 2).[46−49]

$$2NH_4H_2PO_4(S) \rightarrow (NH_4)_2H_2P_2O_7(S) + H_2O(g) \quad (1)$$

$$NH_4H_2PO_4(S) \rightarrow NH_3(g) + H_3PO_4(l) \quad (2)$$

(ii) AZ reacted with H_2O under phosphoric acid catalysis, producing plenty of CO_2 and small amounts of N_2 (reaction 3).

$$3C_2H_4N_4O_2(S) + 6H_2O(g) \xrightarrow{H_3PO_4} 2N_2(g) + 6CO_2(g) + 8NH_3(g) \quad (3)$$

The decreased emission of NH_3 compared to CO_2 can be attributed to the reassociation of NH_3 with phosphoric acid, which was found to be consistent with the previous report by Marcilla et al.[50] Figure 7c displays the photographic evidence of AZ (1.16 g) and H_2O (20 mL) reaction by phosphoric acid catalysis. The samples were prepared with mole ratios of H_3PO_4:AZ = 1:1, H_3PO_4:AZ = 1.5:1, and H_3PO_4:AZ = 2:1. For the sample with a mole ratio of H_3PO_4:AZ = 1:1, the yellow residual AZ particles still could be observed. The decomposition reactions between AZ and H_2O were not performed completely due to the absence of H_2O during the heating process at 120 °C. Conversely, for the samples with mole ratios of H_3PO_4:AZ = 1.5:1 and H_3PO_4:AZ = 2:1, their decomposition reactions between AZ and H_2O could be performed completely. Also, it

https://doi.org/10.1021/acsomega.3c08734
ACS Omega 2024, 9, 5798−5808

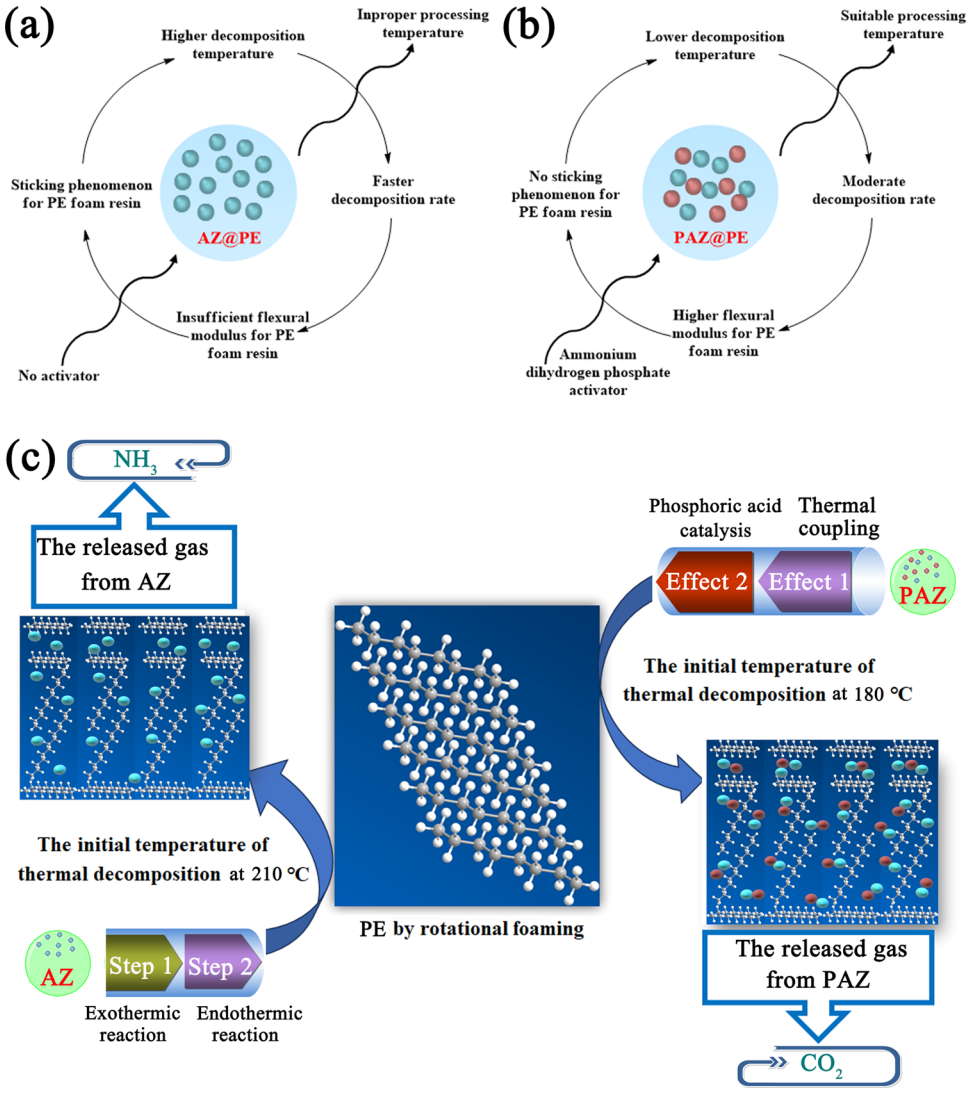

Figure 9. (a) Disadvantages of pure AZ blowing agent. (b) Advantages of PAZ blowing agent. (c) Foaming mechanism comparison of PE foam products by the rotational foaming process with AZ and PAZ, respectively.

was observed that numerous bubbles appeared on the surface of culture dishes, respectively. In fact, the reaction rate gradually accelerated with an increasing amount of phosphoric acid, demonstrating its catalysis effect on the decomposition reaction of AZ with H_2O during the heating process at 120 °C. Furthermore, Figure 7d depicts a scanning electron microscope (SEM) image of the sample with a mole ratio of H_3PO_4:AZ = 1:1 after the decomposition reaction, revealing the formation of numerous bubble pores on its surface (Figure 7e). The corresponding energy-dispersive X-ray spectroscopy (EDS) analysis of the sample in Figure 7d is displayed in Figure 7f. It illustrated that the residual particles comprised C, N, O, and P elements. Considering the initial decomposition temperature of AZ at 210 °C, the above results demonstrated that AZ could react with H_2O by phosphoric acid catalysis.

3.3. Property of PE Foaming Product. It is widely recognized that the foaming behavior of a chemical blowing agent is closely connected to PE foam product properties. To further investigate the properties of the PE foaming product, a comparison was made for PE foam products using pure AZ and the PAZ foaming agent under identical conditions. Three samples of PE foam products were prepared using a twin-screw extruder at a temperature of 135 °C. These samples were labeled as 3.0 wt % AZ@PE, 1.3 wt % AZ@PE, and 3.0 wt % PAZ@PE, respectively. Moreover, the samples of 1.3 wt % AZ@PE and 3.0 wt % PAZ@PE had the same amount of pure AZ. Subsequently, each sample underwent a foaming process in a constant-temperature oven at different temperatures, enabling a comparison of the foaming behavior. The foaming gas amount of 3.0 wt % AZ@PE was relatively small at 180 °C. However, it increased significantly from 180 to 210 °C (Figure S2). The foaming gas amount of 1.3 wt % AZ@PE showed a similar trend (Figure S3). Strikingly, the foaming gas amount of 3.0 wt % PAZ@PE was dramatically large at 180 °C. Additionally, the cell diameter of 3.0 wt % PAZ@PE was smaller compared to the other two samples at 180−210 °C (Figure S4). The density of each foam sample was determined using the immersion method, and the densities at different temperatures are depicted in Figure 8a. Notably, the density of 3.0 wt % PAZ@PE reached its lowest level at 190 °C, and further temperature increase did not cause a significant decline. This suggested that 3.0 wt % PAZ@PE could complete its foaming process at 190 °C, as opposed to the other two samples. The results clearly demonstrate that the foaming temperature of PAZ is dramatically lower than that of AZ. The

https://doi.org/10.1021/acsomega.3c08734
ACS Omega 2024, 9, 5798−5808

histograms in Figure 8b display the cell diameters of 3.0 wt % PAZ@PE, which are significantly smaller than those of the other two samples. This phenomenon can be explained by their different foaming mechanisms. Comparatively, 3.0 wt % PAZ@PE exhibited smaller cell diameters on both the inner and outer surfaces compared with 1.3 wt % AZ@PE. Also, their cell diameter statistics are illustrated in Figure 8c. While the outer surface of 1.3 wt % AZ@PE achieved complete foaming, the inner surface was not fully foamed, showing an average cell diameter of 594 μm. This implies that the cell size of the outer surface in 1.3 wt % AZ@PE is 72% larger than that of the inner surface. In contrast, 3.0 wt % PAZ@PE exhibited complete foaming on both its inner and outer surfaces. Notably, the cell diameter on the outer surface was only slightly larger by about 20% compared to the inner surface. 3.0 wt % PAZ@PE had a more homogeneous cell distribution compared with 1.3 wt % AZ@PE (Figure S5). Concretely, the flexural modulus of the PE foam product is a measure of its ability to withstand deformation caused by bending stress. It plays a significant role in the practical application of PE foam products. Figure 8d shows the flexural properties of the samples. Also, the flexural modulus of 3.0 wt % PAZ@PE was 50% higher than that of 1.3 wt % AZ@PE. This remarkable improvement in the flexural modulus can be attributed to the excellent foaming behavior of the PAZ blowing agent.

Notably, the adherence issue was a major concern during the rotational foaming process of the PE foam products. In the case of the AZ blowing agent, depicted in Figure 8e, there were yellow impurities on the outer surface of the sample, which would detach from the mold surface. This occurrence was attributed to the presence of small amounts of low-molecular compounds, such as biurea, urazol, and cyanic acid.[42,43] These low-molecular-weight compounds had a corrosive effect on the mold and contributed to the sticky molding phenomenon. In contrast, for the PAZ blowing agent, the sticking issue was significantly inhibited. Also, the sample could be effortlessly detached from the mold. The surface had no yellow substance on the surface (Figure 8f). Moreover, the cell size of the PE foam product with the PAZ blowing agent was smaller and more uniform compared to that of the AZ blowing agent (Figures 8g and S3). It indicated that the PAZ blowing agent was significant in ensuring the stable production of high-quality PE foam products during the rotational foaming process.

3.4. Mechanism of the Foaming Behavior for PAZ. For a pure AZ blowing agent, its disadvantages are the higher decomposition temperature and the faster decomposition rate for the PE resin. Therefore, its improper decomposition temperature needs a higher processing temperature, which can lead to uneven cell formation. In fact, the bad foaming behavior of AZ resulted in insufficient flexural modulus and the sticking phenomenon for the PE foam product (Figure 9a). Therefore, a uniquely designed blowing agent of PAZ was obtained by dispersing a small-sized ammonium dihydrogen phosphate activator on the AZ particle surface. Compared with AZ, PAZ achieved a lower decomposition temperature and a moderate decomposition rate, which generated a uniform cell distribution. The excellent foaming behavior improved the flexural modulus and avoided the sticking phenomenon for the PE foam product (Figure 9b). Figure 9c displays the foaming mechanism comparison of AZ and PAZ. AZ had an exothermic reaction first and then an endothermic reaction during thermal decomposition. The initial temperature of thermal decomposition for AZ was nearly 210 °C, which can easily lead to a higher local temperature and result in a higher decomposition rate. The released gas of AZ was mainly NH_3 during thermal decomposition. In contrast, PAZ achieves the active effects of thermal coupling effect and phosphoric acid catalysis. The initial temperature of thermal decomposition for PAZ was nearly 180 °C, which can be beneficial for the PE foam product to obtain a small average cell diameter during the rotational foaming process. Small-sized ammonium dihydrogen phosphate on the AZ surface could be decomposed properly and deliver phosphoric acid and H_2O during the foaming process. Then, AZ reacted with H_2O under phosphoric acid catalysis. Also, this reaction generated CO_2 emission while reducing the emission of NH_3 through recombination with phosphoric acid. The released gas of PAZ was mainly CO_2 due to the significantly tunable foaming behavior.

4. CONCLUSIONS

In this paper, a novel blowing agent for the PE resin was designed and synthesized by a one-pot method. The novel blowing agent PAZ can achieve a lower decomposition temperature and a milder decomposition rate than AZ due to the thermal coupling effect and phosphoric acid catalysis. The PAZ blowing agent generated more small-sized cell nucleation during the thermal decomposition. Also, the fewer thermal decomposition byproducts improved the pretty surface of end-used PE foam products during the rotational foaming process. Compared with pure AZ, PAZ is an excellent blowing agent for the preparation of the PE foam product. The cell diameter of the PE foam product can be reduced significantly using a PAZ blowing agent. Therefore, the flexural modulus of PE foam product produced with PAZ is 50% higher than that produced with pure AZ. Additionally, PAZ, as a blowing agent of PE resin, can provide a better demolding performance and a much more perfect surface than AZ. This work provides an important approach for tuning the foaming behavior of the chemical blowing agent during industrial applications.

■ ASSOCIATED CONTENT

Supporting Information

The Supporting Information is available free of charge at https://pubs.acs.org/doi/10.1021/acsomega.3c08734.

Cell morphology images of all samples (PDF)
AZ, PAZ, dissolved substance of PAZ, and PAZ after DI water washing (PDF)
Images (a−d) 2000 μm (PDF)

■ AUTHOR INFORMATION

Corresponding Authors

Xuelian Chen − *State Key Laboratory of Chemical Resource Engineering, Key Laboratory of Carbon Fiber and Functional Polymers, Ministry of Education, The College of Material Science and Engineering, Beijing University of Chemical Technology, Beijing 100029, China; Shenhua (Beijing) New Materials Technology CO. LTD, CHN Energy Group, Beijing 102211, China;* orcid.org/0000-0001-5518-7683; Email: xuelian.chen@chnenergy.com.cn

Qigu Huang − *State Key Laboratory of Chemical Resource Engineering, Key Laboratory of Carbon Fiber and Functional Polymers, Ministry of Education, The College of Material Science and Engineering, Beijing University of Chemical Technology, Beijing 100029, China;* orcid.org/0000-0002-3367-3557; Email: huangqg@mail.buct.edu.cn

https://doi.org/10.1021/acsomega.3c08734
ACS Omega 2024, 9, 5798−5808

Complete contact information is available at:
https://pubs.acs.org/10.1021/acsomega.3c08734

Notes

The authors declare no competing financial interest.

REFERENCES

(1) Alipour, N.; Andersson, R. L.; Olsson, R. T.; Gedde, U. W.; Hedenqvist, M. S. VOC-Induced Flexing of Single and Multilayer Polyethylene Films As Gas Sensors. *ACS Appl. Mater. Interfaces* **2016**, *8*, 9946−9953.

(2) Marchetti, F.; Palmucci, J.; Pettinari, C.; Pettinari, R.; Marangoni, M.; Ferraro, S.; Giovannetti, R.; Scuri, S.; Grappasonni, I.; Cocchioni, M.; Hodar, F. J. M.; Gunnella, R. Preparation of Polyethylene Composites Containing Silver(I) Acylpyrazolonato Additives and SAR Investigation of their Antibacterial Activity. *ACS Appl. Mater. Interfaces* **2016**, *8*, 29676−29687, DOI: 10.1021/acsami.6b09742.

(3) Byrne, E.; Schaerer, L. G.; Kulas, D. G.; Ankathi, S. K.; Putman, L. I.; Codere, K. R.; Schum, S. K.; Shonnard, D. R.; Techtmann, S. M. Pyolysis-Aided Microbial Biodegradation of High-Density Polyethylene Plastic by Environmental Inocula Enrichment Cultures. *ACS Sustainable Chem. Eng.* **2022**, *10*, 2022−2033.

(4) Lin, Y.; Cao, J.; Zhu, M.; Bilotti, E.; Zhang, H.; Bastiaansen, C. W. M. High-Performance Transparent Laminates Based on Highly Oriented Polyethylene Films. *ACS Appl. Polym. Mater.* **2020**, *2*, 2458−2468, DOI: 10.1021/acsapm.0c00404.

(5) Tian, F.; Decker, E. A.; Goddard, J. M. Development of an Iron Chelating Polyethylene Film for Active Packaging Applications. *J. Agric. Food Chem.* **2012**, *60*, 2046−2052.

(6) Kornberg, A. B.; Thompson, M. R.; Zhu, S. Flexible Conductive Substrate Incorporating a Submicrometer Cocontinuous Polyaniline Phase within Polyethylene by Controlled Crazing. *ACS Appl. Polym. Mater.* **2021**, *3*, 1880−1889.

(7) Minus, M. L.; Chae, H. G.; Kumar, S. Polyethylene Crystallization Nucleated by Carbon Nanotubes under Shear. *ACS Appl. Mater. Interfaces* **2012**, *4*, 326−330.

(8) Zeng, M.; Lee, Y. H.; Strong, G.; LaPointe, A. M.; Kocen, A. L.; Qu, Z.; Coates, G. W.; Scott, S. L.; Abu-Omar, M. M. Chemical Upcycling of Polyethylene to Value-Added α,ω-Divinyl-Functionalized Oligomers. *ACS Sustainable Chem. Eng.* **2021**, *9*, 13926−13936.

(9) Doerr, A. M.; Curry, M. R.; Chapleski, R. C.; Burroughs, J. M.; Lander, E. K.; Roy, S.; Long, B. K. Redox Potential as a Predictor of Polyethylene Branching Using Nickel α-Diimine Catalysts. *ACS Catal.* **2022**, *12*, 73−81.

(10) Liu, X.; Qin, Y.; Zhao, S.; Dong, J. Y. In Situ Promotion of Long-Chain Branching in Polyethylene from Ziegler−Natta Catalysts. *ACS Appl. Polym. Mater.* **2021**, *3*, 6455−6467.

(11) Li, S.; Ju, W.; Sun, W.; Su, Y.; Müller, A. J.; Wang, D. Fractionated Crystallization Behavior of Low-Molecular-Weight Polyethylene Grafted onto SiO_2 Nanoparticles. *ACS Appl. Polym. Mater.* **2022**, *4*, 7841−7851.

(12) Ellis, L. D.; Orski, S. V.; Kenlaw, G. A.; Norman, A. G.; Beers, K. L.; Román-Leshkov, Y.; Beckham, G. T. Tandem Heterogeneous Catalysis for Polyethylene Depolymerization via an Olefin-Intermediate Process. *ACS Sustainable Chem. Eng.* **2021**, *9*, 623−628.

(13) Sharma, V.; Paulbudhe, U.; Bachhar, N.; Chikkali, S. H.; Kumaraswamy, G. Polyethylene-Grafted Sheet-like Silsesquioxane Nanocomposites with Unprecedented Adhesion to Polar Substrates. *ACS Appl. Polym. Mater.* **2023**, *5*, 5972−5983.

(14) Buggy, N. C.; Du, Y.; Kuo, M. C.; Ahrens, K. A.; Wilkinson, J. S.; Seifert, S.; Coughlin, E. B.; Herring, A. M. A Polyethylene-Based Triblock Copolymer Anion Exchange Membrane with High Conductivity and Practical Mechanical Properties. *ACS Appl. Polym. Mater.* **2020**, *2*, 1294−1303.

(15) Lv, Q.; Peng, Z.; Meng, Y.; Pei, H.; Chen, Y.; Ivanov, E.; Kotsilkova, R. Three-Dimensional Printing to Fabricate Graphene-Modified Polyolefin Elastomer Flexible Composites with Tailorable Porous Structures for Electromagnetic Interference Shielding and Thermal Management Application. *Ind. Eng. Chem. Res.* **2022**, *61*, 16733−16746.

(16) Banerjee, R.; Gebrekrstos, A.; Orasugh, J. T.; Ray, S. S. Nanocarbon-Containing Polymer Composite Foams: A Review of Systems for Applications in Electromagnetic Interference Shielding, Energy Storage, and Piezoresistive Sensors. *Ind. Eng. Chem. Res.* **2023**, *62*, 6807−6842.

(17) Yun, S. D.; Lee, C. O.; Kim, H. W.; An, S. J.; Kim, S.; Seo, M. J.; Park, C.; Yun, C. H.; Chi, W. S.; Yeom, S. J. Exploring a New Biocatalyst from Bacillus thuringiensis JNU01 for Polyethylene Biodegradation. *Environ. Sci. Technol. Lett.* **2023**, *10*, 485−492.

(18) Michalak, M.; Hakkarainen, M.; Albertsson, A. C. Recycling Oxidized Model Polyethylene Powder as a Degradation Enhancing Filler for Polyethylene/Polycaprolactone Blends. *ACS Sustainable Chem. Eng.* **2016**, *4*, 129−135.

(19) Wong, A.; Leung, S. N.; Li, G. Y. G.; Park, C. B. Role of Processing Temperature in Polystyrene and Polycarbonate Foaming with Carbon Dioxide. *Ind. Eng. Chem. Res.* **2007**, *46*, 7107−7116.

(20) Kuhnigk, J.; Krebs, N.; Mielke, C.; Standau, T.; Pospiech, D.; Ruckdaschel, H. Influence of Molecular Weight on the Bead Foaming and Bead Fusion Behavior of Poly(butylene terephthalate) (PBT). *Ind. Eng. Chem. Res.* **2022**, *61*, 17904−17914.

(21) Ma, W.; Wu, M.; Gao, P.; Bing, X.; Wu, F.; Wang, L.; Zheng, W. Significantly Improved Foamability and Mechanical Properties of Polypropylene through a Core−Shell Structure via Low Gas Pressure Foam Injection Molding. *Ind. Eng. Chem. Res.* **2023**, *62*, 6149−6157, DOI: 10.1021/acs.iecr.2c04162.

(22) Roy, J. C.; James, L. T. *Rotational Molding Technology*; Plastics Design Library, U.S., 2001; pp 289−290.

(23) Maziers, E. Skin-Foam-Skin TP-Seal Rotomolded Structures: A New Concept for the Production of Car Bodies for Urban Mobility. *Plast. Eng.* **2013**, *69*, 40−42, DOI: 10.1002/j.1941-9635.2013.tb01072.x.

(24) Chen, X.; Huang, Q. Improved Rotational Foam Molding Properties of Tailored Polyethylene Blends with Higher Crystallization Temperature and Viscosity-Temperature Sensitivity. *Polymers* **2022**, *14*, 3486.

(25) Abu, S.; Ben, T.; Robert, C.; Kamran, T.; Lei, W. An Investigation of Low Velocity Impact Properties of Rotationally Molded Skin-Foam-Skin Sandwich Structure. *Polym. Eng. Sci.* **2019**, *60*, 387−397, DOI: 10.1002/pen.25294.

(26) Pop-Iliev, R.; Park, C. B. Single-Step Rotational Foam Molding of Skin-Surrounded Polyethylene Foams. *J. Cell. Plast.* **2003**, *39*, 49−58.

(27) Roberto, C. V.; Luis, C. R.; Francisco, J. M.; Eduardo, M.; Pedro, O.; Rubén, G.; Denis, R. Preparation and Characterization of Multilayer Foamed Composite by Rotational Molding. *Polym. Eng. Sci.* **2015**, *56*, 278−286, DOI: 10.1002/pen.24253.

(28) Pop-Iliev, R. Processing of Integral-Skin Cellular Polymeric Composites in Rapid Rotational Foam Molding. *Acta Phys. Polym., A* **2011**, *120*, 292−297.

(29) Liu, S.-J.; Yang, C.-H. Rotational Molding of Two-layered Polyethylene Foams. *Adv. Polym. Technol.* **2001**, *20*, 108−115.

(30) Werner, J.; Vetter, L.; Hertle, S. Air Inclusions in the Polymer Melt Functioning as Intrinsic Physical Blowing Agents for the Generation of Foams in Rotational Molding. *Cell. Polym.* **2021**, *40*, 3−19, DOI: 10.1177/0262489320920070.

(31) Liu, J.; Qin, S.; Wang, G.; Zhang, H.; Zhou, H.; Gao, Y. Batch Foaming of Ultra-high Molecular Weight Polyethylene with Supercritical Carbon Dioxide: Influence of Temperature and Pressure. *Polym. Test.* **2021**, *93*, No. 106974.

(32) Dong, N. *Study of Fundamental Foaming Mechanisms in Chemical-blowing-agent Based Foaming Process*; National Library of Canada: C.A., 2004.

(33) Maryam, E.; Elizabeth, T.; Michael, R. T.; John, V.; Eric, M. Visual Studies of Model Foam Development for Rotational Molding Processes. *Adv. Polym. Technol.* **2013**, *32*, E809−E821, DOI: 10.1002/adv.21323.

(34) Maryam, E.; Michael, R. T.; John, V. Bubble nucleation in nonpressurized polymer foaming systems. *Polym. Eng. Sci.* **2013**, *54*, 1201−1210, DOI: 10.1002/pen.23658.
(35) Maryam, E.; Michael, R. T.; John, V. Experimental and numerical studies on bubble dynamics in nonpressurized foaming systems. *Polym. Eng. Sci.* **2013**, *54*, 1947−1959, DOI: 10.1002/pen.23737.
(36) Maryam, E.; John, V.; Michael, R. T.; Eric, M. Examining the Influence of Production Scale on the Volume Expansion Behavior of Polyethylene Foams in Rotational Foam Molding. *Adv. Polym. Technol.* **2015**, *34*, 1−8, DOI: 10.1002/adv.21507.
(37) Shahi, P.; Behravesh, A. H.; Rasel, S.; Rizvi, G.; Pop-Iliev, R. Morphological Analysis of Foamed HDPE/LLDPE Blends by X-ray Micro-Tomography: Effect of Blending, Mixing Intensity and Foaming Temperature. *Cell. Polym.* **2017**, *36*, 221−250.
(38) Xu, D.; Pop-Iliev, R.; Park, C. B.; Fenton, R. G. Fundamental Study of CBA-blown Bubble Growth and Collapse Under Atmospheric Pressure. *J. Cell. Plast.* **2005**, *41*, 519−538.
(39) Liu, G.; Park, C.; Lefas, J. Production of low-density LLDPE foams in rotational molding. *Polym. Eng. Sci.* **1998**, *38*, 1997−2009.
(40) Archer, E.; Harkin-Jones, E.; Kearns, M. P.; Crawford, R. J.; Fatnes, A. M. An Investigation of the Rotational Moulding of Foamed Metallocene Polyethylenes. *Rotation* **2002**, *11*, 27−29.
(41) Yamsaengsung, W.; Sombatsompop, N. Effect of chemical blowing agent on cell structure and mechanical properties of EPDM foam, and peel strength and thermal conductivity of wood/NR composite-EPDM foam laminates. *Composites, Part B* **2009**, *40*, 594−600.
(42) Guo, R. L.; Liu, S. H.; Lu, Y. M. Investigation of how pressure influences the thermal decomposition behavior of azodicarbonamide. *J. Loss Prevent. Proc.* **2023**, *83*, No. 105062.
(43) Robledo-Ortiz, J. R.; Zepeda, C.; Gomez, C.; Rodrigue, D.; González-Núñez, R. Non-isothermal decomposition kinetics of azodicarbonamide in high density polyethylene using a capillary rheometer. *Polym. Test.* **2008**, *27*, 730−735.
(44) Nesterenko, A. M.; Savitskas, V. I.; Polumbrik, O. M.; Markovskii, L. N. Quantum-chemical study of electronic structure and enthalpy of decomposition of azodicarbonamide. *Theor. Exp. Chem.* **1983**, *18*, 480−484.
(45) Reyes-Labarta, J. A.; Olaya, M. M.; Marcilla, A. DSC Study of Transitions Involved in Thermal Treatment of Foamable Mixtures of PE and EVA Copolymer with Azodicarbonamide. *J. Appl. Polym. Sci.* **2006**, *102*, 2015−2025.
(46) Torijano, E.; Vargas, R.; Diosa, J.; Mellander, B. E. High temperature phase transitions of $NH_4H_2PO_4$. *Phys. Status Solidi* **2000**, *220*, 659−662.
(47) Lim, A. R.; Lee, K. S. High-temperature behavior of $NH_4H_2PO_4$ studied by single-crystal and MAS NMR. *Solid State Sci.* **2013**, *21*, 54−58.
(48) Abdel-Kader, A.; Ammar, A. A.; Saleh, S. I. Thermal behaviour of ammonium dihydrogen phosphate crystals in the temperature range 25−600 °C. *Thermochim. Acta* **1991**, *176*, 293−304.
(49) Cheng, R. H.; Yen, C. C.; Shern, C. S.; Fukami, T. Studies of high-temperature phase transition, electrical conductivity, and dielectric relaxation in $NH_4H_2PO_4$ single crystal. *J. Appl. Phys.* **2005**, *98*, No. 044104, DOI: 10.1063/1.2009074.
(50) Marcilla, A.; Beltran, M. I.; Gómez-Siurana, A.; Martinez-Castellanos, I.; Berenguer, D.; Pastor, V.; García, A. N. TGA/FTIR study of the pyrolysis of diammonium hydrogen phosphate−tobacco mixtures. *J. Anal. Appl. Pyrolysis* **2015**, *112*, 48−55.

https://doi.org/10.1021/acsomega.3c08734
ACS Omega 2024, 9, 5798−5808